CORE
Metadata, citation and similar papers at core.ac.uk
Provided by IntechOpen

We are IntechOpen, the world's leading publisher of Open Access books Built by scientists, for scientists

4,800
Open access books available

122,000
International authors and editors

135M
Downloads

Our authors are among the

154
Countries delivered to

TOP 1%
most cited scientists

12.2%
Contributors from top 500 universities

WEB OF SCIENCE™

Selection of our books indexed in the Book Citation Index in Web of Science™ Core Collection (BKCI)

Interested in publishing with us?
Contact book.department@intechopen.com

Numbers displayed above are based on latest data collected.
For more information visit www.intechopen.com

Chapter 19

Copper-based Perovskite Design and Its Performance in CO_2 Hydrogenation to Methanol

Feng Li, Haijuan Zhan, Ning Zhao and Fukui Xiao

Additional information is available at the end of the chapter

http://dx.doi.org/10.5772/61520

Abstract

Three series of perovskite-type catalysts, i.e., La–M–Mn–Cu–O (M = Mg, Y, Zn, Ce), La–M–Cu–Zn–O (M = Ce, Mg, Zr, Y), and La–Mn–Zn–Cu–O, were designed and applied in CO_2 hydrogenation to methanol. The materials were characterized by XRD, N_2-adsorption, N_2O-adsorption, ICP-OES, XPS, and TPD techniques. Perovskite structures were observed and the ''metal on oxide'' could be realized via reduction. Upon the introduction of the fourth elements, more structure defects, smaller particles, higher Cu dispersion, larger amount of hydrogen desorption at low temperature, and more amount of basic sites were obtained. The selectivity for methanol and the TOF values were higher for the catalysts derived from perovskite-type precursors. The catalytic performance was related to $Cu^{\alpha+}$ and/or Cu^0 species, low-temperature H_2 adsorption on the unit, and the weak basic sites.

Keywords: Perovskite, Copper, CO_2, Methanol, Hydrogenation

1. Introduction

Perovskite-type oxides have received significant attention because of their important electric, magnetic, ferromagnetic, pyroelectric, and piezoelectric properties [1,2]. Recently, much attention has been paid to perovskite-type oxides as catalysts due to their high activity and thermal stability. For a typical ABO_3 perovskite, A-site is a larger rare earth and/or alkaline earth cation and B-site is a smaller transition metal cation. In such structure, the A-site keeps the structure and the B-site provides the catalytic activity site. B-site cations could be reduced to well-dispersed metallic species supported on the A-site cations oxide, which leads to ideal catalyst precursors for many reactions that involve metal as active sites [3,4]. Besides, perovskite-type A_2BO_4 mixed oxides with the K_2NiF_4 structure, consisting of alternating layers of

INTECH
open science | open minds

© 2016 The Author(s). Licensee InTech. This chapter is distributed under the terms of the Creative Commons Attribution License (http://creativecommons.org/licenses/by/3.0), which permits unrestricted use, distribution, and reproduction in any medium, provided the original work is properly cited.

ABO_3 perovskite and AO rock salt, have also been studied [5], which exhibit variable oxygen stoichiometry. The replacement of A-site and/or B-site cations by other metal cations often results in the formation of crystal microstrain and adjustable activity [6].

CO_2 is the main greenhouse gas, and various strategies have been implemented to reduce its concentration [7-10]. An important CO_2 utilization is the hydrogenation to methanol, which is considered as the most valuable product since it can be used as solvent, alternative fuel, and raw material, and it can be converted to olefins, aromatics, or gasoline derived from traditional petrochemical processes [11,12].

The synthesis of methanol over Cu/ZnO-type catalysts has been studied for many years. However, several important problems still remain open, such as the working oxidation of copper and the reaction mechanism [13-15]. In addition, the low activity and stability of catalysts, which are partly attributed to Cu sintering accelerated by the presence of the by-product, water vapor, create major barriers for practical application [16]. It is found that the catalysts with higher Cu dispersion, easier reduction property, and better adsorption properties for relative gases could achieve better catalytic performance for methanol synthesis [16].

Few work on the application of Cu-based perovskite-type oxides for CO_2 hydrogenation has been investigated. In the present work, three series of perovskite-type-based catalysts were prepared and tested for CO_2 hydrogenation to methanol, and the relationship between physical–chemical property and catalytic performance was discussed.

2. Catalyst preparation

The perovskite-type oxides were prepared by sol-gel method using citric acid as complexing agent. The precursor salts were $La(NO_3)_3$. nH_2O; $Mn(NO_3)_2$, 50% solution; $Cu(NO_3)_2$. $3H_2O$; $Mg(NO_3)_2$. $6H_2O$; $Y(NO_3)_3$. $6H_2O$; $Zn(NO_3)_2$. $6H_2O$; $Ce(NO_3)_3$. $6H_2O$; $ZrO(NO_3)_2.2H_2O$. Adequate amounts of the precursor salts along with citric acid were dissolved in deionized water at a molar ratio of 2:1 (metal cations: citric acid). The solution was heated to 353 K to remove the water, and then the temperature was increased to 423 K until ignition. The resulting powder was finally calcined under air at 673 K for 2 h and then at 1073 K for 4 h. The three series of catalysts were: (1) For doped La–M-Mn–Cu–O based (M= Mg, Y, Zn, Ce) perovskite materials, the ratio for La, M, Mn, Cu is 0.8: 0.2: 0.5: 0.5. The La–Mn–Cu–O catalyst and Mg, Y, Zn, Ce doping catalysts were then denoted as P, Mg–P, Y–P, Zn–P, and Ce–P, respectively. (2) A series of La–M-Cu–Zn–O (M= Ce, Mg, Zr, Y) based perovskite-type catalysts, i.e., $LaCu_{0.7}Zn_{0.3}O_x$, $La_{0.8}Ce_{0.2}Cu_{0.7}Zn_{0.3}O_x$, $La_{0.8}Mg_{0.2}Cu_{0.7}Zn_{0.3}O_x$, $La_{0.8}Zr_{0.2}Cu_{0.7}Zn_{0.3}O_x$ and $La_{0.8}Y_{0.2}Cu_{0.7}Zn_{0.3}O_x$ samples were prepared, of which the subscripts were the nominal composition. The catalysts were then denoted as LCZ-173, LCCZ-8273, LMCZ-8273, LZCZ-8273 and LYCZ-8273, respectively. (3) The $LaZn_{0.4}Cu_{0.6}O_y$, $LaMn_{0.1}Zn_{0.3}Cu_{0.6}O_y$, $LaMn_{0.2}Zn_{0.2}Cu_{0.6}O_y$, $LaMn_{0.3}Zn_{0.1}Cu_{0.6}O_y$, and $LaMn_{0.4}$ $Cu_{0.6}O_y$ samples were prepared, of which the subscripts were the nominal composition. The catalysts were denoted as LZC-046, LMZC-136, LMZC-226, LMZC-316, and LMC-406, respectively.

http://dx.doi.org/10.5772/61520

3. Results and discussion

3.1. Performance of the La–M-Mn–Cu–O (M = Mg, Y, Zn, Ce) based perovskite precursors

3.1.1. Textural and structural properties

As shown in Figure 1a [17], for the La–M-Mn–Cu–O (M = Mg, Y, Zn, Ce) based perovskite precursors, the $LaMnO_3$ (JCPDS # 75-0440) are the main phase. The diffraction peak at about 2θ=32.5° shift towards higher values when the fourth elements were doped. Small peaks at 2θ=35.6°and 38.9°assigned to CuO (JCPDS # 89-5899) appear in the doped samples but not in the P sample. In all diffraction patterns, no phase that ascribes to Mg, Y, or Zn is observed, while a new phase ascribed to CeO_2 is found for the sample of Ce–P, which demonstrates that it is difficult for all the Ce to enter the perovskite lattice, which agrees with the conclusion by Weng et al. [18].

For all reduced samples (Figure 1b), $LaMnO_3$ phase is still the main phase, which reveals that the reduction process does not destroy the perovskite structure. Meanwhile, the CuO phase disappears and the Cu phase emerges.

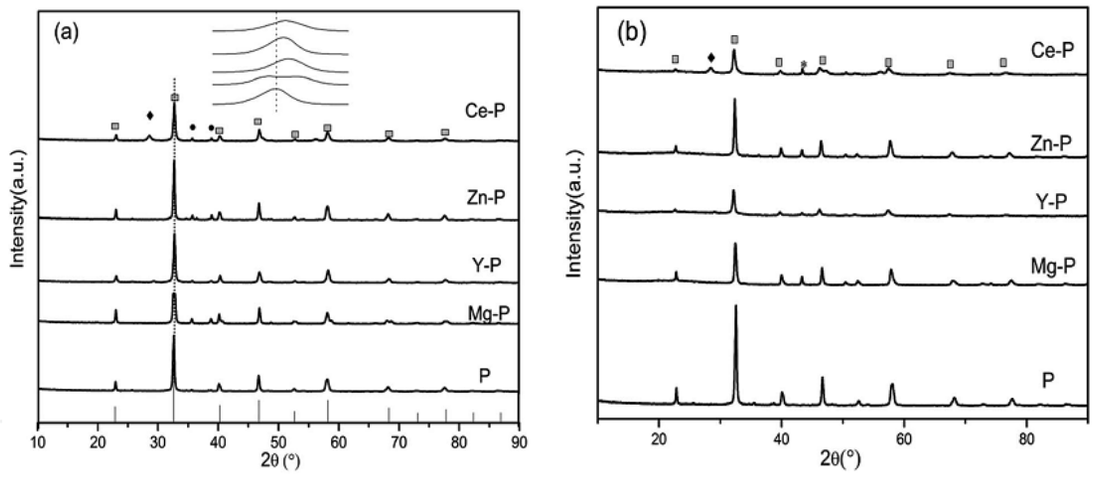

Figure 1. XRD patterns of the calcined (a) and reduced (b) perovskite-type catalysts: (□) $LaMnO_3$; (●) CuO; (◆) CeO_2; (*) Cu (taken from ref.17, reproduced by permission of The Royal Society of Chemistry).

The physicochemical properties of the calcined perovskite-type catalysts are summarized in Table 1 [17]. Low specific surface area for perovskite-type oxides is common. For this series samples, the largest one is only 11.3 $m^2 g^{-1}$ for Y–P and the lowest one is only 4.1 $m^2 g^{-1}$ for the Zn–P. The exposed Cu surface area and the Cu dispersion measured by N_2O adsorption technique are also low, which even cannot be measured for both P and Ce–P. Y–P possesses the largest Cu surface area and the Cu dispersion by comparison. The lower copper surface area may not be favorable for the conversion of CO_2 to methanol [19]. The ICP results show that the experimental lanthanum amount is lower than the theoretical value, and other element amounts are similar to the nominal values.

Samples	S_{BET} ($m^2 g^{-1}$)	Dispersion (%)[a]	S_{Cu} ($m^2 g^{-1}$)	Elemental composition (ICP-OES)[b]
P	6.5	-	-	$La_{0.84}Mn_{0.51}Cu_{0.50}$
Mg-P	5.4	0.9	1.2	$La_{0.67}Mg_{0.22}Mn_{0.49}Cu_{0.50}$
Y-P	11.3	3.8	4.6	$La_{0.67}Y_{0.23}Mn_{0.47}Cu_{0.50}$
Zn-P	4.1	0.7	0.9	$La_{0.67}Zn_{0.18}Mn_{0.50}Cu_{0.50}$
Ce-P	7.2	-	-	$La_{0.68}Ce_{0.19}Mn_{0.49}Cu_{0.50}$

[a] Calculated from N_2O dissociative adsorption.

[b] Subscripts came from ICP results.

Table 1. The physiochemical properties of the perovskite-type catalysts (taken from ref.17, reproduced by permission of The Royal Society of Chemistry).

3.1.2. The XPS investigations

The XPS results presented in Table 2 [17] show that lanthanum ions of the reduced perovskite-type catalysts are present in the trivalent form because the $La_{3d5/2}$ peak is close to the value of pure lanthana at 834.4 eV [20]. However, the BE of $La_{3d5/2}$ of P sample is higher than the other samples, which implies the increasing of the electron cloud density around La ions for the doped samples. It may due to the fourth elements affect the transfer of the electrons of La to O, since O has the highest electronegativity value among all elements [21]. For O_{1s}, the binding energy at around 528.9–529.1 eV is assigned to the lattice oxygen (O^{2-}) [21,22] and the binding energy at around 530.8–533.0 eV is ascribed to the adsorbed oxygen species (O_{ad}) in the surface, which contains hydroxyl (OH^-), carbonate species (CO_3^{2-}), and molecular water. The binding energy decreases after the fourth element except Ce adding, which indicates that there are more electrons around oxygen. It is likely that the fourth components transfer the electronic to the oxygen. The presence of surface adsorbed oxygen species suggests the formation of oxygen vacancies in the defected oxides [23], which is favorable for the activation of the catalyst. The O_{ad}/O^{2-} ratio is increased for the doped samples, which implies the improvement of catalysis activity. The binding energy values of $Mn_{2p3/2}$ for the perovskite-type catalysts are located at 641.3 eV–642.2 eV. The peak positons of level of MnO, Mn_2O_3, and MnO_2 are 640.6, 641.9, and 642.2 eV, respectively. The values are very similar, and the mean oxidation state of Mn ions at the surface layers is extremely difficult to detect by XPS, as reported in other studies [24,25]. However, the previous reports suggested that the BE difference between $Mn_{2p3/2}$ and O_{1s} emissions increases with about 0.6–0.7 eV for the change of the oxidation state between Mn^{3+} and Mn^{4+}. As shown in Table 2, the BE difference is in the range of 112.3–113.0 eV, i.e., increasing with 0.7 eV, which means a change of the Mn^{4+}/Mn^{3+} ratio for the perovskite-type catalysts [26,27].

Since the binding energy of the $Cu_{2p3/2}$ band in the metal (932.6 eV) and in Cu^+ (932.4 eV) is almost same, they can be distinguished by different kinetic energy of the Auger Cu LMM line position in Cu^0 (918.6 eV), Cu^+ (916.7 eV), or in Cu^{2+} (917.9 eV) [19,28]. The Auger electron spectroscopies of Cu LMM of reduced samples are shown in Figure 2 [17]. The profiles are convoluted into two peaks. It can be seen that the majority of the copper species exist as Cu^+

http://dx.doi.org/10.5772/61520

for all samples, which is in accordance with the report of Jia et al. [29]. The weak Cu^0 peak could be the explanation for the immeasurable of exposed Cu^0 for P and Ce–P (Table 1).

The binding energy of the fourth components shows that they exist in Mg-O binding [29], Zn-O binding [23], Y^{3+}, and Ce^{4+}, respectively.

Samples	$La_{3d5/2}$(eV)	$Mn_{2p3/2}$ (eV)	O_{1s} (eV)	O_{ad}/O^{2-}
P	835.1	642.2	529.2 (50.5%)	1.02
			531.7 (49.5%)	
Mg-P	834.0	642.0	529.1 (51.5%)	1.06
			531.5 (48.5%)	
Y-P	834.4	641.3	529.0 (54.0%)	1.18
			531.4 (46.0%)	
Zn-P	834.1	641.5	529.1 (51.2%)	1.05
			531.5 (48.8%)	
Ce-P	834.3	641.8	529.2 (51.9%)	1.08
			532.2 (48.1%)	

Table 2. The binding energy of La, Mn, O, and the ratio of different oxygen species (taken from ref. 17, reproduced by permission of The Royal Society of Chemistry).

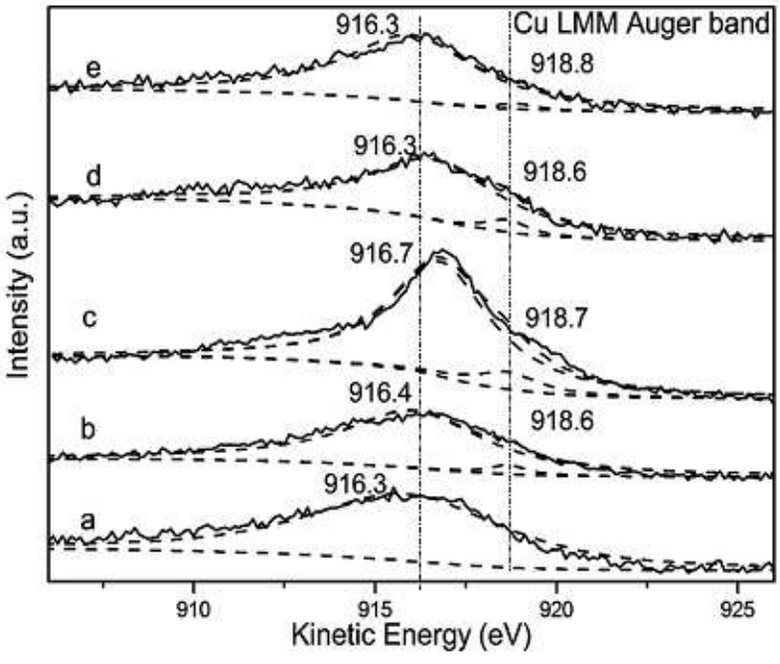

Figure 2. Cu LMM Auger electron spectroscopy of (a) P; (b) Mg–P; (c) Y–P; (d) Zn–P; (e) Ce–P samples after reduction (taken from ref. 17, reproduced by permission of The Royal Society of Chemistry).

3.1.3. H_2-TPD and CO_2-TPD analysis

The H_2 desorption over the prereduced materials on the unit surface area below 523 K (test temperature) increases apparently with the addition of the fourth element, as shown in Table 3 [17].

Two CO_2 desorption peaks are observed for all samples (Figure 3), which are denoted as peak α and peak β [17]. The peak α at around 400 K could be assigned to weak basic sites and the peak β at around 600 K could be assigned to strong basic sites. With the introduction of the fourth components, the peak α shifts to higher temperature, while the peak β shifts to lower temperature, which indicate the increase of the weak basic sites' strength but the decrease of the strong basic sites' strength. The strength for the weak basic sites of the catalysts increases in the order of: P < Ce–P < Y–P < Mg–P < Zn–P. The amount of the basic sites is also changed with the fourth element doping. The quantitative analysis for the CO_2-TPD based on the relative area of the profiles is listed in Table 3, in which the P sample is assigned as 1.00. Both the weak basic sites and the strong basic sites increase due to the alkalinity of Mg for Mg–P. For Y–P, the amount of total basic sites and strong basic sites improved remarkably with the amount of weak basic sites' decreasing. Moreover, the amount of the weak basic sites increases, but the amount of the strong basic sites and total basic sites decrease for Zn–P and Ce–P samples.

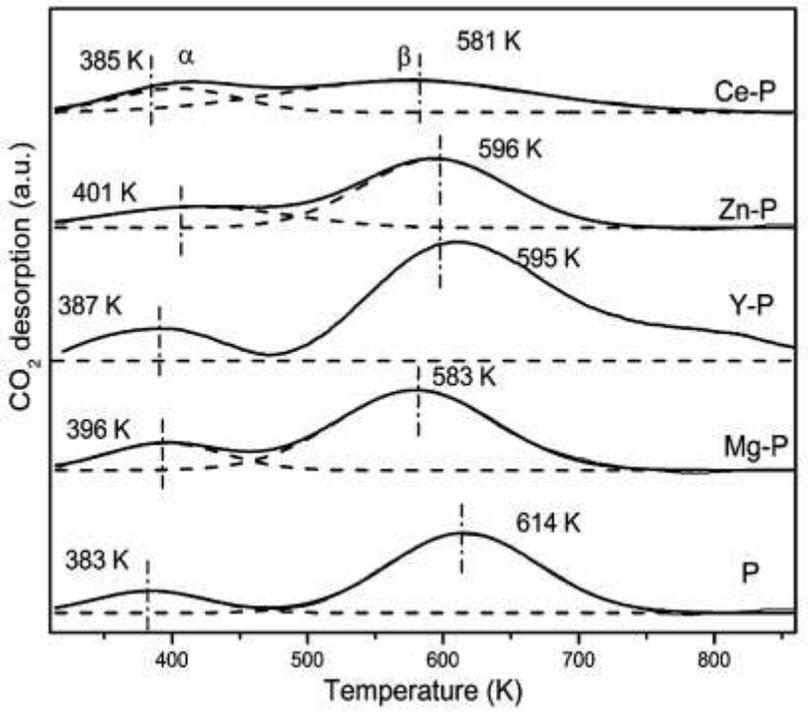

Figure 3. CO_2-TPD curves of the catalysts (taken from ref. 17, reproduced by permission of The Royal Society of Chemistry).

http://dx.doi.org/10.5772/61520

Samples	H_2 desorption below 523 K on per unit area (μmol $g^{-1}m^{-2}$)	Adsoption type and distribution based in CO_2-TPD data[a]		
		Peak α	Peak β	Total
P	1.34	1.00 (383)	1.00 (614)	1.00
Mg-P	3.50	1.30 (396)	1.06 (583)	1.11
Y-P	3.56	0.87 (387)	1.67 (595)	1.53
Zn-P	5.93	1.56 (401)	0.85(596)	0.97
Ce-P	3.47	1.22 (385)	0.69(581)	0.78

[a] The amount of basicity of P is assigned as 1.00 to compare with other samples and the values in parentheses are the desorption temperature (K).

Table 3. The H_2-TPD and CO_2-TPD data (taken from ref. 17, reproduced by permission of The Royal Society of Chemistry).

3.1.4. Catalytic performance

The catalytic performances of the catalysts for CO_2 hydrogenation to methanol are summarized in Table 4 [17]. Both the CO_2 conversion and methanol selectivity are improved when the fourth element is added. With the introduction of Zn, the activity increased greatly, which might be due to the fact that the active site is $Cu^{\delta+}$–O–Zn^{2+} [31,32]. However, the activity improvement is slight for Ce-P. The relationship between the CO_2 conversion and the amount of H_2 desorption on unit surface area below 523 K (Table 3) is shown in Figure 4 [17]. It can be seen that the more the H_2 that is desorbed on the unit area, the more the CO_2 that is converted. Lower CO_2 conversion may result from lower copper content as well as lower surface area of copper in the system. The results of Figure 5 [17] show that the trend of the weak basic sites' strength and methanol selectivity is similar, which indicates their dependency.

Samples	CO_2 conversion (%)	Selectivity (C-mol%)		
		CH_3OH	CO	CH_4
P	1.8	0.7	93.4	5.9
Mg-P	2.8	23.7	68.1	6.5
Y-P	4.6	14.5	82.6	2.9
Zn-P	6.1	51.0	46.4	2.7
Ce-P	2.0	5.0	85.9	9.2

Reaction conditions: $n(H_2)/n(CO_2)$=3:1, T=523 K, P=5.0 MPa, GHSV=4000 h^{-1}.

Table 4. The performance for methanol synthesis from CO_2 hydrogenation over the reduced catalysts (taken from ref. 17, reproduced by permission of The Royal Society of Chemistry).

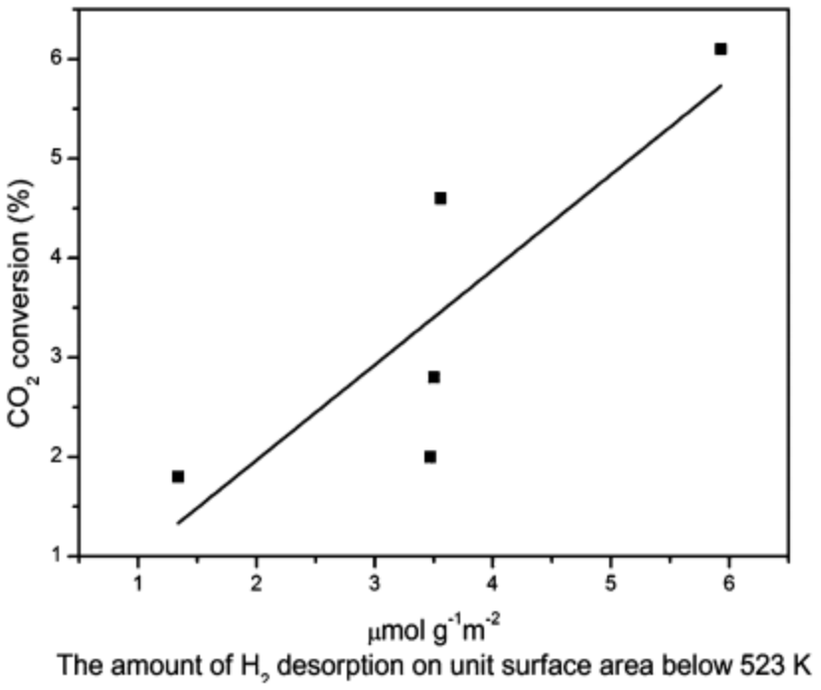

Figure 4. Relationship between the CO_2 conversion and the amount of H_2 desorbed on unit surface area below 523 K (taken from ref. 17, reproduced by permission of The Royal Society of Chemistry).

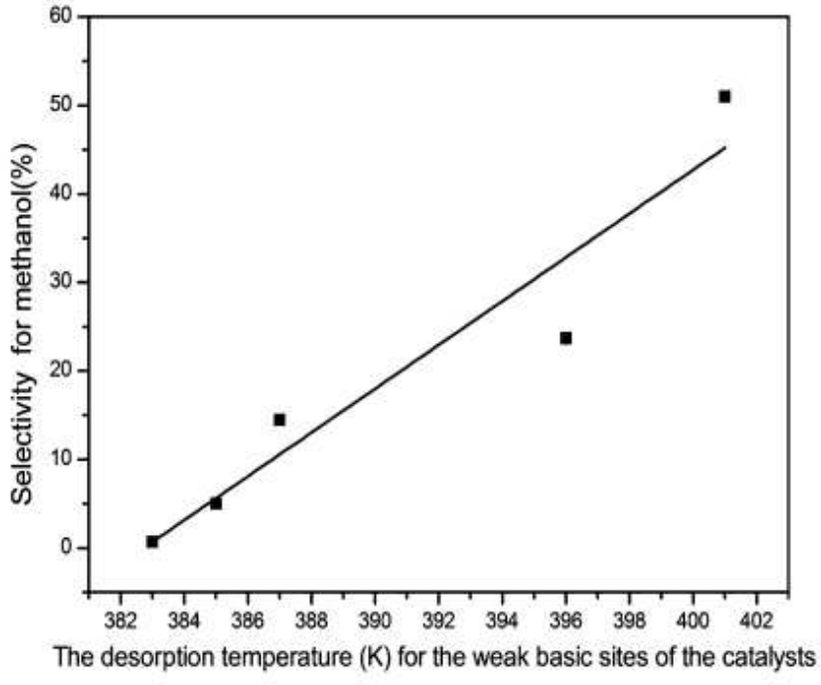

Figure 5. Relationship between the selectivity for methanol and the strength of the weak basic sites of the catalysts (taken from ref.17, reproduced by permission of The Royal Society of Chemistry).

http://dx.doi.org/10.5772/61520

3.2. Performance of the La-M-Cu-Zn-O (M = Ce, Mg, Zr, Y) based perovskite precursors

3.2.1. Textural and structural properties

Figure 6 [33] shows that the orthorhombic perovskite structure (A_2BO_4) with high degree of crystallinity of the La_2CuO_4 (JCPDS # 82-2142) is the main phase and two small peaks at 2θ=35.6° and 38.9° ascribed to the CuO phase (JCPDS # 89-5899) present in all samples. The weak peak at 2θ=36.3° attributed to the ZnO phase (JCPDS # 80-0075) appears in all samples except LMCZ-8273, which implies that Mg seems to have a special effect on the structure. The phase of Ce_7O_{12} and $La_2Zr_2O_7$ appear in the sample of LCCZ-8273 and LZCZ-8273, respectively, while there are no new phases containing Mg and Y appearing in the sample of LMCZ-8273 and LYCZ-8273.

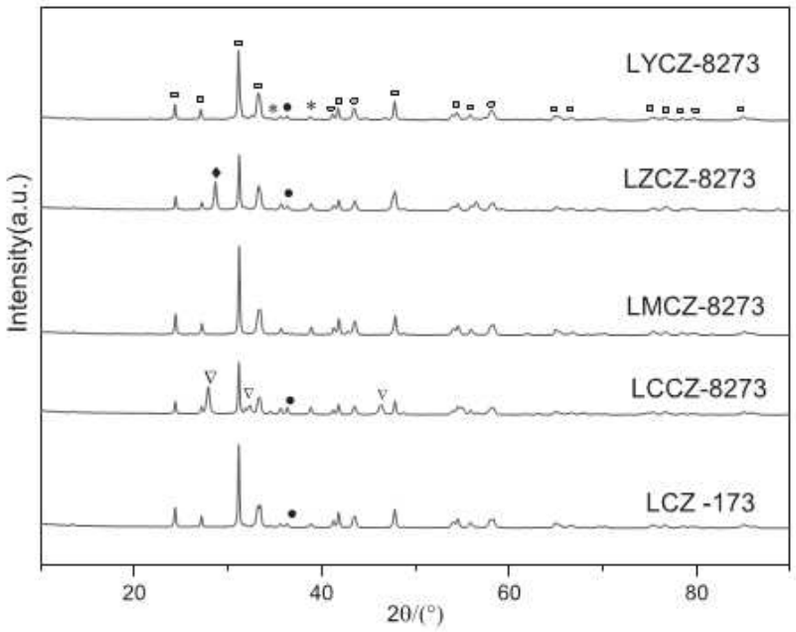

Figure 6. XRD patterns of the perovskite-type catalysts: (□)La_2CuO_4; (*)CuO; (◆)$La_2Zr_2O_7$; (●)ZnO; (∇)Ce_7O_{12} (taken from ref. 33, reproduced by permission of Elsevier B.V.)

The crystallographic parameters of the prepared materials were calculated by employing least-squares refinement, assuming an orthorhombic crystal system for the samples, and the results are listed in Table 5 [33]. A certain degree of changes of the lattice parameters occured after the fourth component was introduced. The lattice parameters a, b, and c were lower than those of LCZ-173, which can be attributed to the shrinkage of the La_2CuO_4 due to the introduction of the fourth elements. The mean grain size of La_2CuO_4 calculated by the Scherrer equation shows that the particles size of the La_2CuO_4 decreased remarkably for LCCZ-8273, LZCZ-8273, and LMCZ-8273, but slightly for LYCZ-8273. The physicochemical properties of the calcined catalysts are summarized in Table 6 [33]. The BET surface area for all calcined samples are rather low ($S_{BET} < 3\ m^2\ g^{-1}$), which is common for perovskite-type of materials [4]. It can be seen that the highest specific surface area is just only 2.3 $m^2\ g^{-1}$ for LZCZ-8273. Moreover, the

tendency of the exposed Cu surface area and the Cu dispersion measured by N_2O adsorption is the same for the materials. The LZCZ-8273 shows the highest Cu surface area (S_{Cu}) and the best dispersion of copper (D_{Cu}). The physicochemical properties of LYCZ-8273 are similar to that of the LCZ-173, which indicates that the influence of the Y doping is negligible.

Samples	Lattice parameters (Å)			Volume (Å^3)	Size of La_2CuO_4 crystallites (nm)
	a	*b*	*c*		
LCZ-173	5.365	5.409	13.170	383.8	95.6
LCCZ-8273	5.350	5.392	13.137	381.8	31.9
LMCZ-8273	5.352	5.400	13.157	380.6	22.5
LZCZ-8273	5.356	5.404	13.149	379.0	24.0
LYCZ-8273	5.359	5.363	13.127	377.3	84.5

Table 5. The lattice parameters of the perovskite-type catalysts (taken from ref. 33, reproduced by permission of Elsevier B.V.).

Samples	S_{BET} (m^2g^{-1})	Dispersion[a] (%)	S_{Cu} (m^2g^{-1})
LCZ-173	0.7	5.3	3.4
LCCZ-8273	1.3	8.5	5.9
LMCZ-8273	1.2	8.5	6.2
LZCZ-8273	2.3	8.6	6.5
LYCZ-8273	0.7	4.5	3.2

[a] Calculated from N_2O dissociative adsorption.

Table 6. The physiochemical properties of the perovskite-type catalysts (taken from ref. 33, reproduced by permission of Elsevier B.V.).

3.2.2. XPS investigations

The reduced perovskite-type catalysts are analyzed by XPS, and the binding energies (BE) of $La_{3d5/2}$ and $Zn_{2p3/2}$ are presented in Table 7 [33]. According to the literature, $La_{3d5/2}$ features in perovskite structure are located at 837.5 and 834.3 eV [20,34] which are close to the values of pure lanthana at 837.8 and 834.4 eV, indicating that lanthanum ions are present in the trivalent form. A slight shift in the $La_{3d5/2}$ binding energy is observed upon introduction of the fourth elements and the values are in the range of 837.86–838.01 eV and 834.06–834.36 eV, respectively. Small differences may relate to the changes in crystal structure and/or electronic structure. In addition, small changes are also observed for the binding energy of Zn at around 1021.7 eV for different samples. The Auger electron spectroscopies of Cu LMM of reduced samples are shown in Figure 7 [33]. A broad peak appears in the range of 915.0 eV–920.0 eV for all samples, and it is hard to distinguish the Cu^+, Cu^{2+}, and Cu^0 apparently. However, the peaks at around

http://dx.doi.org/10.5772/61520

918.6 eV attributed to Cu^0 are distinct for all samples. A new peak appears at around 911.2–914.3 eV, lower than that of Cu^+, which is defined as peak α, implying that a special Cu species $Cu^{\alpha+}$ exists in the perovskite system. The presence of Cu^+ may accelerate the reduction of CO_2 to CO (RWGS) [34],while the $Cu^{\alpha+}$ (not Cu^{2+}, Cu^+, Cu^0) plays an important role for the methanol synthesis from CO_2/H_2 [31,35].

The X-ray photoelectron spectroscopies of the fourth elements in the reduced samples suggest that both Ce^{3+} and Ce^{4+} exist in the LCCZ-8273 and the +4 oxidation state is predominant. The result agrees with the XRD analysis. The Zr in the LZCZ-8273 sample exists in the phase of $La_2Zr_2O_7$.

Samples	Binding energy (eV)	
	La $_{3d5/2}$	Zn $_{2p3/2}$
LCZ-173	837.89 834.15	1021.67
LCCZ-8273	837.92 834.06	1021.71
LMCZ-8273	837.87 834.36	1021.34
LZCZ-8273	838.01 834.26	1021.78
LYCZ-8273	837.86 834.23	1021.69

Table 7. XPS parameters of the perovskite-type catalysts (taken from ref. 33, reproduced by permission of Elsevier B.V.).

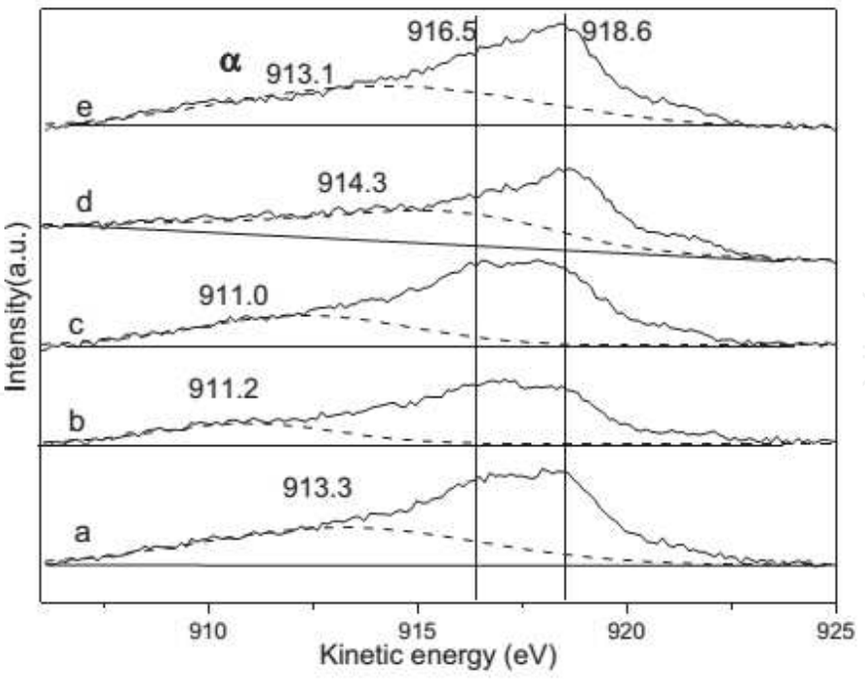

Figure 7. Cu LMM Auger electron spectroscopy of (a) LCZ-173; (b) LCCZ-8273; (c) LMCZ8273; (d) LZCZ-8273; (e) LYCZ-8273 samples after reduce (taken from ref. 33, reproduced by permission of Elsevier B.V.).

3.2.3. Catalytic performance

The catalytic performance for La-M-Cu-Zn-O (M = Ce, Mg, Zr, Y) catalysts are listed in Table 8 [33]. The LMCZ-8273 shows the highest CO_2 conversion and the maximum yield of methanol despite the lowest selectivity among all the samples. The LMCZ 8273 shows the highest methanol selectivity and the LCCZ-8273 shows moderate CO_2 conversion and methanol selectivity. The lowest CO_2 conversion and less improvement for methanol selectivity are observed for LYCZ-8273. The varying of the CO_2 conversion had the same tendency as the surface area of copper (Figure 8 [33]), indicating more surface copper existing in the catalysts may lead to higher activity, i.e., Cu^0 is the active site for CO_2 hydrogenation to methanol [10,16,19,22,35]. It is noteworthy that all catalysts show promising CH_3OH selectivity, especially for LMCZ-8273. The order of the selectivity to CH_3OH is as follows: LMCZ-8273 > LCCZ-8273 > LYCZ-8273 > LCZ173 > LZCZ-8273. The relationship between CH_3OH selectivity and the $Cu^{\alpha+}$ Auger peaks is shown in Figure 9 [33]. It can be seen that $Cu^{\alpha+}$ had a strong effect on the selectivity for methanol: the lower the binding energy of the peak α, the higher is the CH_3OH selectivity. Cu^+ is favorable for the reduction of CO_2 to CO (RWGS), so it can be derived that the farther away from 916.6 eV (the binding energy of Cu^+ in Cu LMM) for the peak α, the higher the CH_3OH selectivity that can be obtained. As discussed above, doping of Mg leads to the proper oxide state of copper, which results in the best selectivity for methanol. For LCCZ-8273 and LYCZ-8273, Ce and Y substitute La in the A-site with the same charge (+3) and similar ionic radius, which produces more defects in the perovskite structure that causes the special oxide state for copper species. With the special structure of La_2CuO_4 perovskite, the high dispersed copper species can be realized and stronger physical and electric interaction between the copper and other metal oxides can be obtained, which may lead to the formation and stabilization of the copper species with special valence [23]. However, for the LZCZ-8273, the formation of lanthanum zirconium pyrochlore has little influence on the perovskite structure but a great influence on the content of La_2CuO_4 perovskite, which may lead to the lowest selectivity of methanol. The turnover frequency (TOF), which represents the number of CO_2 molecules hydrogenated in a unit site per second (s^{-1}), is calculated from the exposed copper surface area for the perovskite-type catalysts (Table 8 [33]). The TOF values of the perovskite-type catalysts were very high compared with other catalytic systems [22,35], indicating the better efficiency for copper atoms on perovskite-type catalysts.

Samples	CO_2 conversion (%)	Selectivity (C-mol%)			CH_3OH yield (g $gcat^{-1}$ h^{-1})	TOF(Cu) × 10^3 (s^{-1})
		CH_3OH	CO	CH_x		
LCZ-173	6.4	57.9	39.5	2.5	0.05	65.1
LCCZ-8273	8.1	63.3	34.9	1.7	0.08	48.9
LMCZ-8273	9.1	65.2	33.0	1.8	0.09	52.0
LZCZ-8273	12.6	52.5	46.0	1.4	0.10	68.0
LYCZ-8273	5.0	59.6	37.0	3.5	0.04	55.7

Reaction conditions: $n(H_2)/n(CO_2)$=3:1, T=523 K, P=5.0 MPa, GHSV=3600 h^{-1}.

Table 8. Catalytic performance for methanol synthesis from CO_2 hydrogenation over the reduced catalysts (taken from ref. 33, reproduced by permission of Elsevier B.V.).

http://dx.doi.org/10.5772/61520

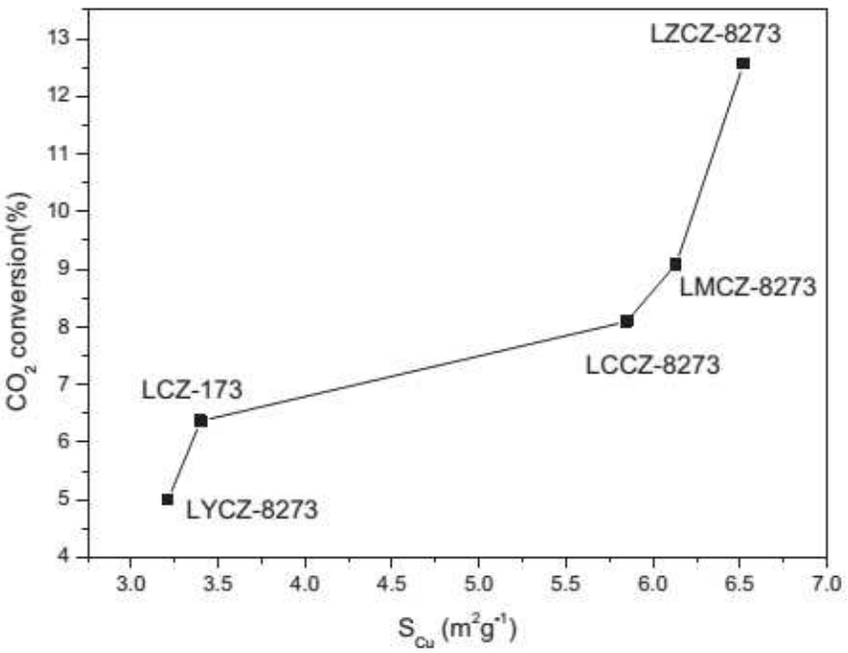

Figure 8. Relationship between copper surface area and CO_2 conversion (taken from ref. 33, reproduced by permission of Elsevier B.V.).

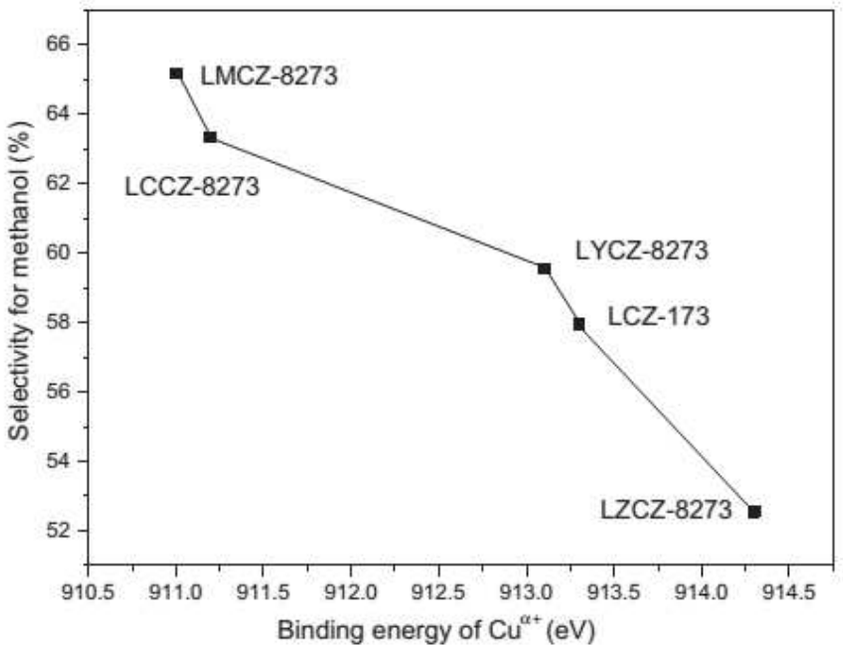

Figure 9. Relationship between methanol selectivity and the binding energy of $Cu^{\alpha+}$ (taken from ref. 33, reproduced by permission of Elsevier B.V.).

3.3. Performance of the La–Mn–Zn–Cu–O based perovskite precursors

3.3.1. Textural and structural properties

The XRD patterns of the fresh and reduced perovskites are presented in Figure 10a and b, respectively [36]. La_2CuO_4 perovskite-like structure can be observed for all fresh samples. $LaMnO_3$ phase emerges and the La_2CuO_4 phase transfers from tetragonal (JPCDS 81-2450) to orthorhombic (JPCDS 81-0872) as the manganese is introduced, which indicates that the manganese introduction distorts the structure of the La_2CuO_4. With the increasing of the manganese amount, the intensity of the La_2CuO_4 phase decreases while that of the $LaMnO_3$ phase increases, which implies that the formation of $LaMnO_3$ is easier than that of La_2CuO_4. This phenomenon reveals that the structure of $LaMnO_3$ is more stable than La_2CuO_4. Small peaks for both CuO and ZnO can also be observed except LMC-046, which indicates the perovskite structure has certain tolerance for the involved elements for this perovskite-type system. Moreover, the peak intensity of the separated CuO decreases when the value of Mn/Zn decreases, which means the formation of $LaMnO_3$ can lead to the separation of copper from the La_2CuO_4 perovskite structure. For the reduced sample (Figure 10b), the La_2CuO_4 perovskite structure disappears and the metallic copper and La_2O_3 is observed, which indicates that the ''metal-on-oxide'' can be attained. The appearance of $La_{0.974}Mn_{0.974}O_3$ phase reveals that the reduction progress can result in defects rather than destruction for the Mn-based perovskite.

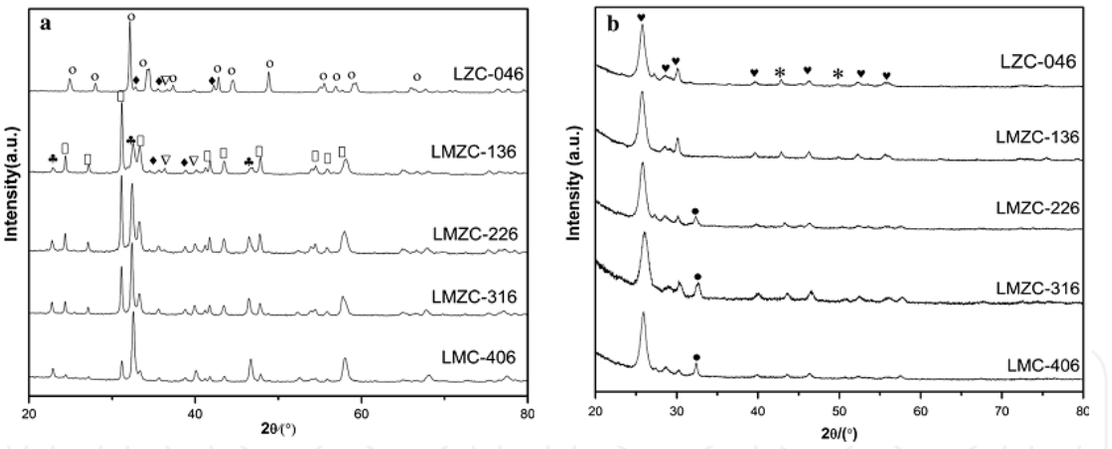

Figure 10. X-ray patterns of the fresh (a) and reduced (b) catalysts: (o) tetragonal La_2CuO_4; (□) orthorhombic La_2CuO_4; (▽) CuO; (◆) ZnO; (♣) $LaMnO_3$; (♥) La_2O_3; (•) $La_{0.974}Mn_{0.974}O_3$; (*) Cu (taken from ref. 36, reproduced by permission of Springer Science+Business Media).

The crystallographic parameters of the prepared materials were calculated by employing least-squares refinement and the results are listed in Table 9 [36]. It can be found that the axes are elongated for the four element samples, which means that doping may strut the perovskite structure. The size of La_2CuO_4 crystallites becomes smaller with the introduction of manganese. The $LaMnO_3$ phase changes from cubic to orthorhombic structure as zinc is introduced. Moreover, the LMZC-136 and LZC-046 possess the smallest $LaMnO_3$ and the largest La_2CuO_4

http://dx.doi.org/10.5772/61520

crystallites among all the samples, which implies that the abundant zinc species can improve the formation of small $LaMnO_3$ and large La_2CuO_4 crystallites. The change of lattice parameters of the samples implies that interaction between the involved elements might be different.

The BET specific surface area along with the exposed surface copper area and the copper dispersion measured by N_2O adsorption are summarized in Table 10 [36]. The specific surface area for all samples is low, which is common for perovskite-type materials [37]. LMC-406 possesses the largest specific surface area (S_{BET}), the exposed surface copper area (S_{Cu}) as well as the copper dispersion (D_{Cu}), while the LZC-046 sample shows the lowest S_{Cu} and D_{Cu}, which indicate that the existence of $LaMnO_3$ perovskite structure is favorable for increasing the surface copper area due to the extension of the space structure for the samples with manganese (Table 9).

Samples	Lattice parameters of $LaMnO_3$ (Å)			Size of $LaMnO_3$ crystallites (Å)	Lattice parameters La_2CuO_4 (Å)			Size of La_2CuO_4 crystallites (Å)
	a	*b*	*c*		*a*	*b*	*c*	
LZC-046	-	-	-	-	3.696	3.696	12.770	841
LMZC-136	5.472	7.754	5.513	224	5.352	5.400	13.157	820
LMZC-226	5.502	7.774	5.521	356	5.350	5.393	13.137	825
LMZC-316	5.472	7.751	5.513	475	5.350	5.393	13.157	831
LMC-406	3.88	3.88	3.88	352	5.351	5.395	13.139	658

Table 9. The lattice parameters of the perovskite-type samples (taken from ref. 36, reproduced by permission of Springer Science+Business Media).

Samples	**S_{BET} ($m^2\ g^{-1}$)**	**Dispersion[a] (%)**	**S_{Cu} ($m^2\ g^{-1}$)**
LZC-046	2.4	1.9	2.3
LMZC-136	1.1	2.3	2.7
LMZC-226	1.4	2.6	2.8
LMZC-316	1.2	2.7	3.0
LMC-406	2.5	4.2	4.5

[a] Calculated from N_2O dissociative adsorption.

Table 10. The physiochemical properties of the perovskite-type catalysts (taken from ref. 36, reproduced by permission of Springer Science+Business Media).

3.3.2. XPS investigations

The XPS results of the reduced perovskite-type catalysts are listed in Table 11 [36]. The values of $La_{3d5/2}$ binding energy (BE) are located in the range of 834.2–834.6 eV, demonstrating that La ions are in the trivalent form for all samples. Small changes of Zn (around 1021.7 eV) and Mn (around 642.0 eV) BE may relate to the small distortions in electronic structure and/or crystal

structure. For the O_{1s} patterns, the peak at around 528.2–529.3 eV can be attributed to the oxygen ions in the crystal lattice (O^{2-}) and the peak at around 531.1–531.5 eV can be assigned to the adsorbed oxygen species (O_{ad}) derived from the defects or oxygen vacancies in the structure [38]. The O_{1s} BE shifts to lower value with the decreasing of the Mn/Zn ratio, which suggests the increasing of electron cloud density around O element. The value of O_{ad}/O^{2-} is max for the LZC-046, which decreases for the Mn containing samples, indicating that the $LaMnO_3$ could reduce the structural defects.

For this series catalyst, the binding energies of $Cu_{2p3/2}$ are lower than that for the copper oxide (933.0 eV) apparently, indicating that the Cu atoms are not in the simple copper oxides form. Figure 11 [36] shows the Auger electron spectroscopies of Cu LMM for the reduced samples. A broad peak can be observed, which can then be deconvoluted into three peaks. The peak at around 916.5 and 919.0 eV matched with kinetic binding energy of Cu^{+} and Cu^{0} within the error limit, respectively. However, a new peak at around 911.2–913.2 eV is observed which may be ascribed to the $Cu^{\alpha+}$. According to literatures and our works, $Cu^{\alpha+}$ can be appeared in perovskite-type system.

Samples	Binding energy (eV)					
	$La_{3d5/2}$	$Cu_{2p3/2}$	$Mn_{2p3/2}$	$Zn_{2p3/2}$	O_{1s}	O_{ad}/O^{2-}
LZC-046	834.6	932.2	-	1021.4	528.2	1.33
					531.1	
LMZC-136	834.3	932.4	642.0	1021.8	528.7	1.29
					531.3	
LMZC-226	834.2	932.5	641.9	1021.6	528.8	1.25
					531.3	
LMZC-316	834.3	932.7	642.0	1021.6	529.2	1.18
					531.4	
LMC-406	834.5	932.6	642.0	-	529.3	1.13
					531.5	

Table 11. XPS data of the perovskite-type catalysts (taken from ref. 36, reproduced by permission of Springer Science +Business Media).

3.3.3. Catalytic performance

The performance of the La–Mn–Zn–Cu–O based perovskite catalysts for methanol synthesis from CO_2 hydrogenation is shown in Table 12 [36]. The LMC-406 shows the worst performance despite the largest surface area and exposed copper surface area. The LZC- 046, which also contains three metal elements, but Zn instead of Mn, shows a moderate catalytic performance. It is well-known that the site of Cu^{+}-O-Zn^{2+} favors the adsorption of hydrogen that can transport to the bulk copper species via spillover [20,39]. So the lack of the site of Cu^{+}-O-Zn^{2+} may be the reason for the poor catalytic performance of LMC-406. Moreover, the TOF_{Cu} value increases sharply upon Zn introduction, which verifies that the copper sites are not the only active sites

http://dx.doi.org/10.5772/61520

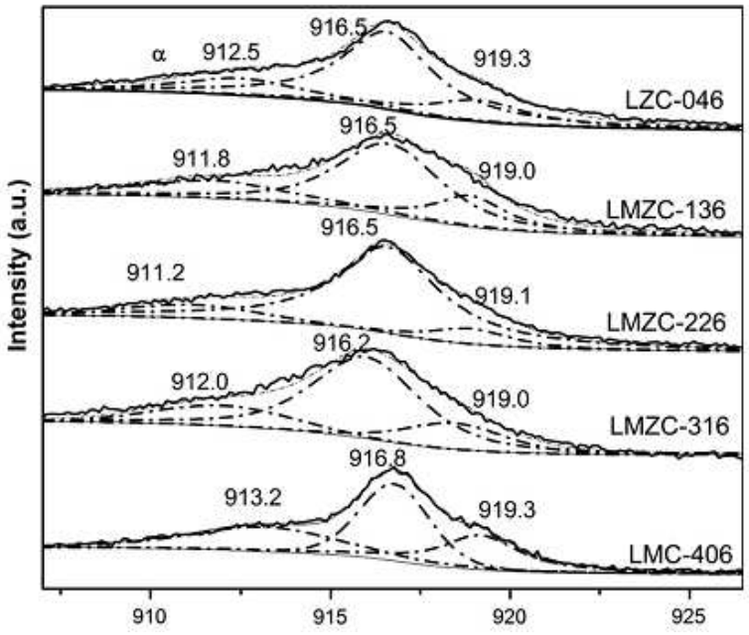

Figure 11. Cu LMM Auger electron spectroscopy of the reduced perovskite-type catalysts (taken from ref. 36, reproduced by permission of Springer Science+Business Media).

for the reaction [40]. With more reducible copper species and high TOF_{Cu} values, the four-component samples show a good catalytic performance. The ratio of both $Cu^{\alpha+}$ and Cu^0 species to the total copper species (calculated from the Auger spectroscopy (Figure 11)) shows the same change tendency with the CO2 conversion (Figure 12) [36], indicating that both $Cu^{\alpha+}$ and Cu^0 species could be the active sites for the conversion of CO_2. In addition, with the change of the ratio for Mn/Zn, the synergy between copper and the other components might vary, and then the reduction state of copper species ($Cu^{\alpha+}$ and Cu^0) changes. The four-component samples with two kinds of perovskites show better methanol selectivity, which implies that the strong synergy for different elements and different perovskite phases are significant for the improvement of the catalytic performance. In addition, it is also found that the lower the BE of the $Cu^{\alpha+}$, the higher is the CH_3OH selectivity (Figure 13) [36].

Samples	CO_2 conversion (%)	Selectivity (C-mol%)			CH_3OH yield ($g\ gcat^{-1}h^{-1}$)	$TOF_{Cu} \times 10^3$ (s^{-1})	$(Cu^{\alpha+}+Cu^0)/Cu_{Total}$(%)[a]
		CH_3OH	CO	CH_x			
LZC-046	11.0	48.2	50.4	1.3	0.07	129.4	55.31
LMZC-136	10.1	54.2	44.2	1.5	0.07	104.3	54.41
LMZC-226	10.7	55.3	43.3	1.4	0.08	161.1	54.93
LMZC-316	13.1	54.5	44.5	1.1	0.10	121.5	56.82
LMC-406	7.9	27.2	70.7	2.1	0.03	35.5	54.06

[a] The ratio value was calculated from the Auger spectroscopy (Figure 11).

Reaction conditions: $n(H_2)/n(CO_2)$ = 3:1, T = 543 K, P = 5.0 MPa, GHSV = 3800 h^{-1}.

Table 12. The catalytic performance for methanol synthesis from CO_2 hydrogenation over the reduced catalysts (taken from ref. 36, reproduced by permission of Springer Science+Business Media).

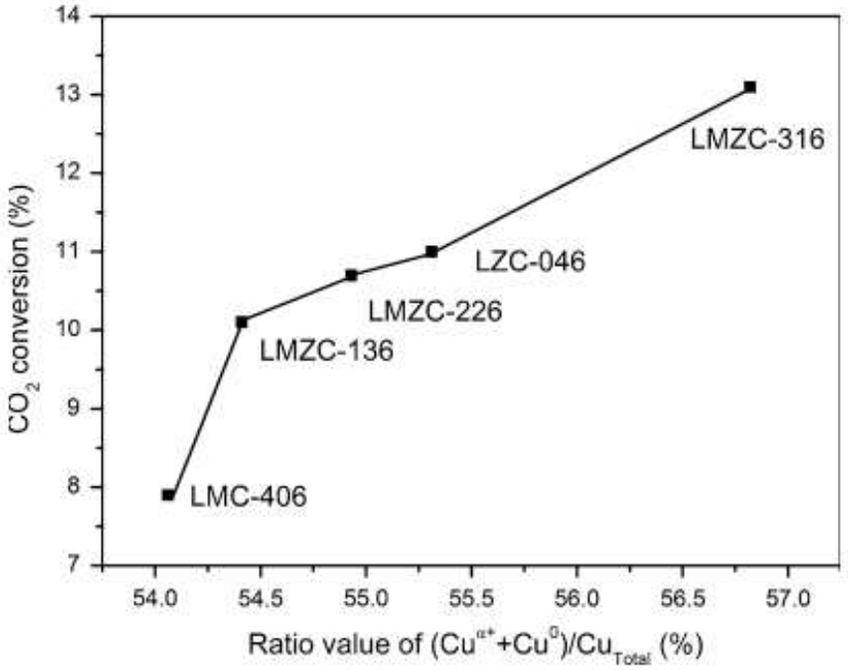

Figure 12. Relationship between CO_2 conversion and ratio value of $(Cu^{\alpha+}+Cu^0)/Cu_{Total}$ (taken from ref.36, reproduced by permission of Springer Science+Business Media).

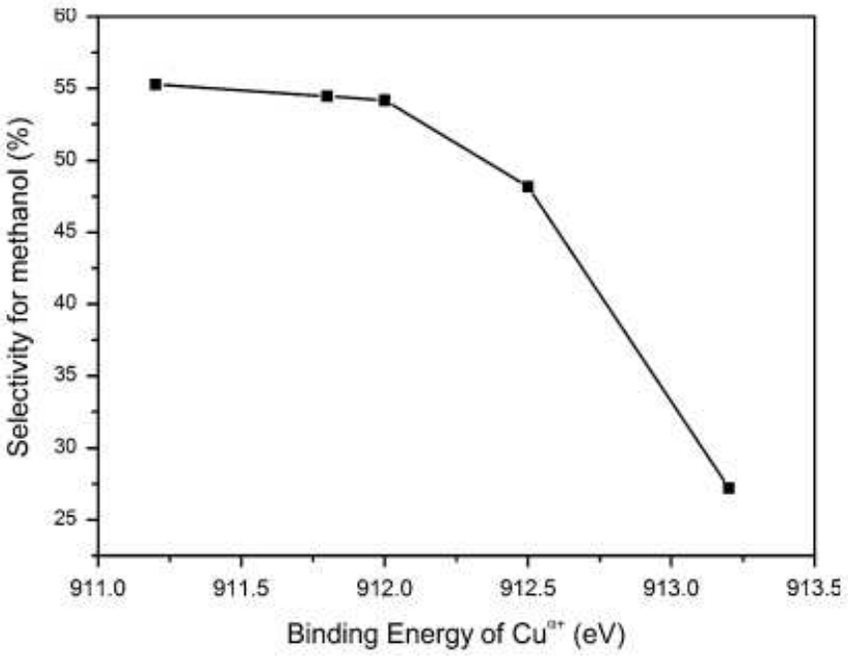

Figure 13. Relationship between methanol selectivity and binding energy of $Cu^{\alpha+}$ (taken from ref. 36, reproduced by permission of Springer Science+Business Media).

4. Conclusions

Three series of catalysts derived from perovskite-type precursors were prepared by sol-gel method, which were applied in the CO_2 hydrogenation to methanol. The conclusions are as follows:

1. The perovskite-type ABO_3, A_2BO_4, and ABO_3+A_2BO_4 can be purposive obtained in our work. Cu-based perovskite-type catalyst shows good methanol selectivity in CO_2 hydrogenation to methanol.
2. For La–M–Mn–Cu–O (M = Mg, Y, Zn, Ce) catalysts, the introduction of the fourth elements leads to the separation of copper from the $LaMnO_3$ perovskite lattice and thus produces more oxygen vacancies. Because of the increasing of defects, temperature adsorption properties are improved for the doped samples. The CO_2 conversion is related to the amount of absorbed H_2 on the unit area under 523 K, and the methanol selectivity corresponds to the strength of the weak basic sites. The catalytic performance enhanced considerably for Zn–P based on this, which also implies that Zn is important to the CO_2 hydrogenation to methanol.
3. La_2CuO_4 (A_2BO_4) perovskite structure is obtained for the La–M–Cu–Zn–O (M = Ce, Mg, Zr, Y) samples. With the addition of Ce, Mg, and Zr, good properties can be obtained: smaller particle size, higher Cu dispersion, larger amount of hydrogen desorption at low temperature, higher concentration of basic sites, and so on. The excellent methanol selectivity originates from the special copper valence that presents in the perovskite structure after reduction, and the CO_2 conversion is in correlation with the surface area of metallic copper.
4. Both La_2CuO_4 and $LaMnO_3$ perovskite structure can be observed in the $LaMn_{0.4-x}Zn_xCu_{0.6}O_y$ (x = 0, 0.1, 0.2, 0.3, 0.4) catalysts. The ''metal-on-oxide'' can be realized after reduction. With decreasing of Mn/Zn, more oxygen defects were formed. The perovskites exhibited better methanol selectivity due to the appearance of $Cu^{\alpha+}$ derived from the abundant defects of perovskite structure and the strong interaction between different elements. Moderate $LaMnO_3$ can balance the defects in the structure, and then lead to the perfect $Cu^{\alpha+}$, which is important for the methanol selectivity.

Acknowledgements

This work was financially supported by the Key Science and Technology Program of Shanxi Province, China (MD2014-10), the National Key Technology Research and Development Program of the Ministry of Science and Technology (2013BAC11B00), and the Natural Science Foundation of China (21343012).

Author details

Feng Li[1*], Haijuan Zhan[2], Ning Zhao[1,3*] and Fukui Xiao[1,3]

*Address all correspondence to: lifeng2729@sxicc.ac.cn; zhaoning@sxicc.ac.cn

1 State Key Laboratory of Coal Conversion, Institute of Coal Chemistry, Chinese Academy of Sciences, Taiyuan, People's Republic of China

2 School of Chemistry and Chemical Engineering, Ningxia University, Yinchuan, People's Republic of China

3 National Engineering Research Center for Coal-based Synthesis, People's Republic of China

References

[1] Tejuca L.G, Fierro J.L.G, Tascón J.M.D. Structure and Reactivity of Perovskite-Type Oxides. *Adv Catalys*. 1989; 36: 237-328. DOI: 10.1016/s0360-0564(08)60019-x

[2] Sun X.F., Komiya S., Ando Y. Anomalous damping of phonon thermal transport in lightly Y- or Eu-doped La_2CuO_4 single crystals. *Physica C*. 2003; 388-389: 355-356. DOI: 10.1016/s0921-4534(02)02500-5

[3] Jia L.s., Gao J., Fang W.p., Li Q.b. Carbon dioxide hydrogenation to methanol over the pre-reduced $LaCr_{0.5}Cu_{0.5}O_3$ catalyst. *Catalys Commun*. 2009; 10: 2000-2003. DOI: 10:2000-2003.10.1016/j.catcom.2009.07.017

[4] Pen˜a M.A., Fierro J.L.G. Chemical structures and performance of perovskite oxides. *Chem Rev*. 2001; 101: 1981-2017. DOI: 10.1021/cr980129f

[5] Zhong H., Zeng R. Structure of $LaSrMO_4$(M = Mn, Fe, Co, Ni, Cu) and their catalytic properties in the total oxidation of hexane. *J Serbian Chem Soc*. 2006; 71: 1049-1059. DOI: 10.2298/jsc0610049z

[6] Riza F., Ftikos C. Influence of A^- and B^-site doping on the properties of the system $La_2CoO_{4\pm\delta}$. *J Eur Cera Soc*. 2007; 27: 571-573. DOI: 10.1016/j.jeurceramsoc.2006.04.069

[7] Li B., Duan Y., Luebke D., Morreale B. Advances in CO_2 capture technology: A patent review. *Appl Energy*. 2013; 102: 1439-1447. DOI: 10.1016/j.apenergy.2012.09.009

[8] Steeneveldt R., Berger B., Torp T.A. CO_2 capture and storage. *Chem Engin Res Design*. 2006; 84: 739-763. DOI: 10.1205/cherd05049

[9] Yu K.M., Curcic I., Gabriel J., Tsang S.C. Recent advances in CO_2 capture and utilization. *ChemSusChem*. 2008; 1: 893-899. DOI: 10.1002/cssc.200800169

[10] Peters M., K°ohler B., Kuckshinrichs W., Leitner W. Chemical technologies for exploiting and recycling carbon dioxide into the value chain. *ChemSusChem*. 2011; 4: 1216-1240. DOI: 10.1002/cssc.201000447

[11] Xu X.d., Moulijn J.A. Mitigation of CO_2 by chemical conversion: plausible chemical reactions and promising products. *Energy Fuels*. 1996; 10: 305-325. DOI:10.1021/ef9501511

[12] Olah G.A. Beyond oil and gas: the methanol economy. *Angewante Chemie*. 2005; 44: 2636-2639. DOI: 10.1002/anie.200462121

[13] Fujita S-i., Kanamori Y., Satriyo A.M, Takezawa N. Methanol synthesis from CO_2 over Cu-ZnO catalysts prepared from various coprecipitated precursors. *Catalysis Today*. 1998; 45: 241-244. DOI: 10.1016/S0920-5861(98)00222-3

[14] Klier K. Methanol synthesis. *Adv Catalys*. 1982; 31: 243-313. DOI: 10.1016/s0360-0564(08)60455-1

[15] Gao L.Z., Au C.T. CO_2 Hydrogenation to methanol on a $YBa_2Cu_3O_7$ catalyst. *JCatalys*. 2000; 189: 1-15. DOI: 10.1006/jcat.1999.2682

[16] Natesakhawat S., Lekse J.W, Baltrus J.P., Ohodnick P.R., Howard B.H., Deng X.Y., Matranga C. Active sites and structure–activity relationships of copper-based catalysts for carbon dioxide hydrogenation to methanol. *ACS Catalysis*. 2012; 2: 1667-1676. DOI: 10.1021/cs300008g

[17] Zhan H.j., Li F., Gao P., Zhao N., Xiao F.k., Wei W., Sun Y.h. Influence of element doping on La–Mn–Cu–O based perovskite precursors for methanol synthesis from CO_2/H_2. *RSC Adv*. 2014; 4: 48888–48896. DOI: 10.1039/c4ra07692c

[18] Weng D., Zhao H.s., Wu X.d., Xu L.h., Shen M.q. Influence of cerium on the performance of $LaMO_{3+\lambda}$ (M = Mn or Mn–Cu) perovskite-type catalyst. *Mater Sci Engin*. 2003; 361: 173-178. DOI: 10.1016/s0921-5093(03)00524-0

[19] Gao P., Li F., Zhan H.j., Ning Z., Xiao F.K, Wei W., Zhong L.S, Wang H., Sun Y.H. Influence of Zr on the performance of Cu/Zn/Al/Zr catalysts via hydrotalcite-like precursors for CO_2 hydrogenation to methanol. *J Catalys*. 2013; 298: 51-60. DOI: 10.1016/j.jcat.2012.10.030

[20] Merino N., Barbero B., Grange P., Cadus L. LaCaCoO perovskite-type oxides: preparation, characterisation, stability, and catalytic potentiality for the total oxidation of propane. *J Catalys*. 2005; 231: 232-244. DOI: 10.1016/j.jcat.2005.01.003

[21] Sutthiumporn K, Kawi S. Promotional effect of alkaline earth over Ni–La_2O_3 catalyst for CO_2 reforming of CH_4: Role of surface oxygen species on H_2 production and carbon suppression. *Int J Hydrogen Energy*. 2011; 36:14435-14446. DOI: 10.1016/j.ijhydene.2011.08.022

[22] Słoczyński J., Grabowski R., Kozłowska A., Olszewski P., Lachowska M., Skrzypek J., Stoch J. Effect of Mg and Mn oxide additions on structural and adsorptive properties

of Cu/ZnO/ZrO_2 catalysts for the methanol synthesis from CO_2. *Appl Catalys A*. 2003; 249: 129-138. DOI: 10.1016/s0926-860x(03)00191-1

[23] Li Z.q., Meng M., Zha Y.q., Dai F.f., Hu T.d., Xie Y.n., Zhang J. Highly efficient multi-functional dually-substituted perovskite catalysts $La_{1-x}K_xCo_{1-y}CuyO_{3-\delta}$ used for soot combustion, NO_x storage and simultaneous NO_x-soot removal. *Appl Catalys B*. 2012; 121-122: 65-74. DOI: 10.1016/j.apcatb.2012.03.022

[24] Rubio-Marcos F., Quesada A., García M.A., Banares M.A., Fierro J.L.G, Martin-Gonzalez M.S., Costa-Kramer J.L., Fernandez J.F. Some clues about the interphase reaction between ZnO and MnO_2 oxides. *J Solid State Chem*. 2009; 182: 1211-1216. DOI: 10.1016/j.jssc.2009.02.009

[25] Kenji Tabata Y.H., Suzuki E. XPS studies on the oxygen species of $LaMn_{1-x}CuxO_{3+\lambda}$. *Appl Catalys A*. 1998; 170: 245–254. DOI: 10.1016/j.molstruc.2014.04.065

[26] Batis N.H., Delichere P., Batis H. Physicochemical and catalytic properties in methane combustion of $La_{1-x}Ca_xMnO_{3\pm y}$ ($0\leq x\leq 1$; $-0.04\leq y\leq 0.24$) perovskite-type oxide. *Appl Catalys A*. 2005; 282: 173-180. DOI: 10.1016/j.apcata.2004.12.009

[27] Najjar H., Batis H. La–Mn perovskite-type oxide prepared by combustion method: Catalytic activity in ethanol oxidation. *Appl Catalys A*. 2010; 383: 192-201. DOI: 10.1016/j.apcata.2010.05.048

[28] Gao P., Li F., Xiao F.K., Zhao N., Sun N.N, Wei W., Zhong L.S, Sun Y.H. Preparation and activity of Cu/Zn/Al/Zr catalysts via hydrotalcite-containing precursors for methanol synthesis from CO_2 hydrogenation. *Catalys Sci Technol*. 2012; 2: 1447. DOI: 10.1039/c2cy00481j

[29] Jia L.s., Gao J., Fang W.p., Li Q.b. Influence of copper content on structural features and performance of pre-reduced $LaMn_{1-x}Cu_xO_3$ ($0\leq x<1$) catalysts for methanol synthesis from CO_2/H_2. *J Rare Earths*. 2010; 28: 747-751. DOI: 10.1016/s1002-0721(09)60193-9

[30] Aykut Y., Parsons G.N, Pourdeyhimi B., Khan S.A. Synthesis of mixed ceramic $Mg_xZn_{1-x}O$ nanofibers via Mg^{2+} doping using sol-gel electrospinning. *Langmuir*. 2013; 29: 4159-4166. DOI: 10.1021/la400281c

[31] Arena F., Italiano G., Barbera K., Bordiga S., Bonura G., Spadaro L., Frusteri F. Solid-state interactions, adsorption sites and functionality of Cu-ZnO/ZrO_2 catalysts in the CO_2 hydrogenation to CH_3OH. *Appl Catalys A*. 2008; 350: 16-23. DOI: 10.1016/j.apcata.2008.07.028

[32] Miller B.J.A., Martin-luengo M.A., Vong M.S.W., Wang Y., Self V.A., Chapmanc S.M, Sermon P.A. Junctions between CuO_x and ZnO_y in sensors for CO and catalysts for CO hydrogenation. *J Mater Chem*. 1997; 7: 2155-2160. DOI: 10.1039/a700747g

[33] Zhan H.j., Li F., Gao P., Zhao N., Xiao F.k., Wei W., Sun Y.h. Methanol synthesis from CO_2 hydrogenation over La-M-Cu-Zn-O(M=Y, Ce, Mg, Zr) catalysts derived from

perovskite-type precursors. *J Power Sources*. 2014; 251: 113-121. DOI: 10.1016/j.jpowsour.2013.11.037

[34] Maluf S.S., Nascente P.A.P., Afonso C.R.M., Assaf E.M. Study of $La_{2-x}Ca_xCuO_4$ perovskites for the low temperature water gas shift reaction. *Appl Catalys A*. 2012; 413-414: 85-93. DOI: 10.1016/j.apcata.2011.10.047

[35] Arena F., Italiano G., Barbera K., Bonura G., Spadaro L., Frusteri F. Basic evidences for methanol-synthesis catalyst design. *Catalys Today*. 2009; 143: 80-85. DOI: 10.1016/j.cattod.2008.11.022

[36] Zhan H.j., Li F., Xin Ch.l., Zhao N., Xiao F.k.,Wei W., Sun Y.h. Performance of the La–Mn–Zn–Cu–O based perovskite precursors for methanol synthesis from CO_2 hydrogenation. *Catalys Lett*. 2015; 145:1177–1185.DOI: 10.1007/s10562-015-1513-8

[37] Gao L.zh., Chua H.T., Kawi S. The direct decomposition of NO over the La_2CuO_4 nanofiber catalyst. *J Solid State Chem*. 2008; 181: 2804-2807. DOI: 10.1016/j.jssc.2008.06.051

[38] Tien-Thao N., Alamdari H., Kaliaguine S. Characterization and reactivity of nanoscale $La(Co,Cu)O_3$ perovskite catalyst precursors for CO hydrogenation. *J Solid State Chem*. 2008; 181: 006-2019. DOI: 6/j.jssc.2007.11.016

[39] Yuan Z.L., Wang L.N., Wang J.H., Xia S.X., Chen P., Hou Z.Y., Zhen X.M. Hydrogenolysis of glycerol over homogenously dispersed copper on solid base catalysts. *Appl Catalys B*. 2011; 101: 431-440. DOI: 6/j.apcatb.2010.10.013

[40] Islam Q.A, Nag S., Basu R.N. Study of electrical conductivity of Ca-substituted $La_2Zr_2O_7$. *Mater Res Bull*. 2013; 48: 103-3107. DOI: 6/j.materresbull.2013.04.081

IntechOpen

IntechOpen

IntechOpen